International Journal of Hydrogen Energy 203 (2026) 152973

Contents lists available at ScienceDirect

International Journal of Hydrogen Energy

journal homepage: www.elsevier.com/locate/he

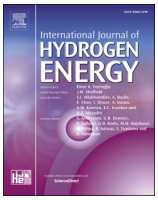

Thermal conductivity of the benzyltoluene-based liquid organic hydrogen carrier system and its hydrogenated and oxygenated derivatives

Hubert P. Blabus [a], Francisco E. Berger Bioucas [a], Michael H. Rausch [a], Thomas M. Koller [a,1,*], Peter Wasserscheid [b,c,d], Andreas P. Fröba [a]

[a] Institute of Advanced Optical Technologies – Thermophysical Properties (AOT-TP), Department of Chemical and Biological Engineering (CBI) and Erlangen Graduate School in Advanced Optical Technologies (SAOT), Friedrich-Alexander-Universität Erlangen-Nürnberg (FAU), Paul-Gordan-Straße 8, 91052 Erlangen, Germany
[b] Forschungszentrum Jülich GmbH, Helmholtz Institute Erlangen-Nürnberg for Renewable Energy (IEK-11), Cauerstraße 1, 91058 Erlangen, Germany
[c] Institute of Chemical Reaction Engineering (CRT), Department of Chemical and Biological Engineering (CBI), Friedrich-Alexander-Universität Erlangen-Nürnberg (FAU), Egerlandstraße 3, 91058 Erlangen, Germany
[d] Forschungszentrum Jülich GmbH, Institute for a Sustainable Hydrogen Economy, Am Brainergy Park 4, 52428 Jülich, Germany

ARTICLE INFO

Keywords:
Autothermal concept
Density
Liquid organic hydrogen carriers
Parallel-plate method
Prediction
Thermal conductivity

ABSTRACT

This work investigates the thermal conductivity λ_c of the benzyltoluene-based liquid organic hydrogen carrier (LOHC) system relevant for autothermal process concepts. Besides the three regioisomers of the dehydrogenated benzyltoluene (H0-BT), their corresponding hydrogenated and partially oxidized derivatives perhydrobenzyltoluene (H12-BT) and methylbenzophenone (oxo-H0-BT) are studied. Using a guarded parallel-plate instrument, λ_c is determined at atmospheric pressure and temperatures between (278.15 and 358.15) K with an expanded relative uncertainty of 2 %. The experimental λ_c data increase from H12-BT via H0-BT to oxo-H0-BT and show no significant influence of regioisomerism for each class. For selected binary H0-BT/H12-BT mixtures, a non-linear behavior for λ_c as a function of amount fraction was found, while λ_c of binary H0-BT/oxo-H0-BT mixtures agrees with the values for the pure substances. An available prediction model for λ_c of cyclic hydrocarbons represents the measurement results for the H0-BT and H12-BT regioisomers reasonably well, yet shows shortcomings in case of the oxo-H0-BT regio-isomer.

1. Introduction

In order to address the challenges in the transition from a fossil fuel-based energy economy towards a sustainable defossilized one, new solutions for energy production and storage are currently considered [1–3]. One promising concept is the liquid organic hydrogen carrier (LOHC) technology [4–10]. Its principle is based on the storage and release of the energy carrier hydrogen (H_2) in reversible cycles of exothermic hydrogenation and endothermic dehydrogenation of a liquid carrier molecule [11]. A recently proposed efficiency-enhancing process step includes the partial oxidation of a certain amount of the dehydrogenated LOHC component to the corresponding oxo-derivative form. This exothermic step releases heat that can be used to supply the energy-intensive dehydrogenation reaction [12]. Using this autothermal process concept, the total amount of released H_2 can be increased by up to 27 % in comparison to the conventional process without partial oxidation considering a constant amount of LOHC material [12]. As stated in the literature [11,13,14], aromatic hydrocarbons seem to be among the most promising classes of LOHC chemicals. Out of this group, the dehydrogenated benzyltoluene (H0-BT) and its hydrogenated counterpart perhydrobenzyltoluene (H12-BT) represent an LOHC pair that has been extensively studied, see, e.g., Refs. [4,10,15–17]. The corresponding partially oxidized species of H0-BT is methylbenzophenone (oxo-H0-BT) which can be converted back to the hydrogenated LOHC via a hydrodeoxygenation step [12].

For the design and modeling of the LOHC process, the thermophysical properties of the associated fluids need to be known at process-relevant conditions. In the case of the BT-based LOHC system, temperatures T between about (400–600) K and pressures p between (0.1 and 7) MPa are typically applied during the hydrogenation, dehydrogenation, and partial oxidation reactions [11,12]. These reactions create mixtures

* Corresponding author.
E-mail addresses: hubert.blabus@fau.de (H.P. Blabus), francisco.bioucas@fau.de (F.E. Berger Bioucas), michael.rausch@fau.de (M.H. Rausch), thomas.m.koller@fau.de (T.M. Koller), peter.wasserscheid@fau.de (P. Wasserscheid), andreas.p.froeba@fau.de (A.P. Fröba).
[1] Present address: Institute of Thermodynamics, Technische Universität Braunschweig, Hans-Sommer-Straße 5, 38106 Braunschweig, Germany

https://doi.org/10.1016/j.ijhydene.2025.152973
Received 1 August 2025; Received in revised form 5 December 2025; Accepted 8 December 2025
Available online 23 December 2025

Abbreviations

AARD	average absolute relative deviation
GC	gas chromatography
GPPI	guarded parallel-plate instrument
H0-BT or BT	benzyltoluene
H6-BT	cyclohexylmethyl-methylbenzene
H12-BT	perhydrobenzyltoluene
H0-DBT	dibenzyltoluene
H18-DBT	perhydrodibenzyltoluene
H0-DPM or DPM	diphenylmethane
H12-DPM	dicyclohexylmethane
HI ERN	Helmholtz-Institut Erlangen-Nürnberg
LOHC	liquid organic hydrogen carrier
m	meta
oxo-H0-BT	methylbenzophenone
oxo-H0-DPM	benzophenone
o	ortho
p	para

whose compositions changes with time. During hydrogenation and dehydrogenation, mixtures of H0-BT, the partially hydrogenated intermediate cyclohexylmethyl-methylbenzene (H6-BT), and H12-BT are found, whereas mixtures of H0-BT and oxo-H0-BT occur during the partial oxidation process [12,17,18]. A further challenge in connection with the BT-system is that it features regioisomerism, i.e. there exist three different regioisomers of H0-BT, namely, H0-ortho-BT (H0-o-BT), H0-meta-BT (H0-m-BT), and H0-para-BT (H0-p-BT), which are typically available in technical mixtures [16]. As a result of the hydrogenation and oxidation of H0-BT, also corresponding regioisomers of H12-BT and oxo-H0-BT will be formed. All these issues impede a detailed characterization of the involved LOHC fluids and their mixtures with respect to their thermophysical properties. One of these is the thermal conductivity λ_c which describes the ability of a material to conduct energy in the form of heat as a result of a T gradient. The hydrogen storage in an LOHC system involves process steps which produce (hydrogenation, partial oxidation in the autothermal concept) or consume heat (dehydrogenation for H_2 release). The proper engineering of the conversion units in which heat removal or heat provision must be realized to enable an effective process critically relies on the knowledge of λ_c of the relevant substances and reaction mixtures under process-relevant conditions. This ensures maintaining suitable reaction conditions within the desired T windows. Moreover, high uncertainties for λ_c due to a poor or even nonexistent database require the need to use safety factors for the reactor design. This results often in oversized reactor units, including heat exchangers, and increased capital costs [19–21]. Thus, accurate knowledge of λ_c is crucial from engineering, economic, and safety-related perspectives. Until now, experimental information on λ_c of hydrocarbon-based LOHCs, including the BT-based system and its hydrogenated and oxygenated derivatives, is very limited. So far, there are only measurement results from a previous study obtained for a technical mixture of H0-BT consisting of the three individual regioisomers, the related H12-BT isomeric mixture, and mixtures of H0-BT and H12-BT at atmospheric p of about 0.1 MPa and T from (298.15–323.15) K [15]. In the same work, λ_c was also determined experimentally for the structurally very similar LOHC candidates diphenylmethane (H0-DPM), a technical mixture of dibenzyltoluene (H0-DBT) as well as the associated hydrogenated forms. However, knowledge about the influence of the regioisomerism on λ_c of the BT-based system and of λ_c of the partially oxygenated oxo-H0-BT itself is still lacking.

The accurate measurement of thermal conductivity in an absolute way with low uncertainties is a challenging task until today [22,23]. Measurements can be performed by transient or steady-state methods [22,24]. The latter have the advantage to rely on relatively simple working equations, which allows for a more straightforward determination of λ_c in comparison to the transient methods. There are two common variants of steady-state methods given by parallel plates or concentric cylinders [24]. The parallel-plate method, which is applied in this work and realized in the form of a guarded parallel-plate instrument (GPPI), can serve as an absolute method for the measurement of λ_c with expanded (coverage factor $k = 2$) relative uncertainties of about (2–3) % [23]. This has been demonstrated for, e.g., various liquids [15,23,25], including the reference materials water and toluene, but also for dispersions with a continuous liquid phase such as nanofluids [26–28] or microemulsions [29,30] at p of about 0.1 MPa and T from (283–363) K. Since measurements for λ_c of liquids cannot be carried out at any conceivable thermodynamic state, corresponding prediction models were developed in the literature. In addition to models which are based on a theoretical background [31,32], empirical correlations connecting λ_c to other thermophysical properties [15,33–36] are often available. One empirical prediction model for λ_c was suggested in a recent work of Berger Bioucas et al. [15], which allowed to represent the T-dependent experimental data for λ_c of selected cyclic hydrocarbons, including technical mixtures of H0-BT and H12-BT, typically within ±5 %.

The aim of the present work is the experimental determination of the thermal conductivity of the BT-based LOHC system relevant for autothermal process concepts. For addressing the influence of regioisomerism on λ_c of the dehydrogenated, hydrogenated, and partially oxygenated substances, the three respective pure regioisomers of H0-BT, H12-BT, and oxo-H0-BT were measured. To mimic the changing fluid composition during the hydrogenation, dehydrogenation, and oxidation steps, selected binary mixtures of H0-BT/H12-BT and H0-BT/oxo-H0-BT containing a common isomeric type were also studied. Here, the technically most relevant para- or ortho-regioisomers were selected since they often represent the major components in commonly available technical BT-based mixtures [37,38]. All measurements for λ_c were performed at T between (278.15 and 358.15) K in steps of 10 K at atmospheric pressure using a GPPI. This T range represents the range where the measurement instrument can reliably be operated with low expanded uncertainty of about 2 %. Although this low-T region studied experimentally is below the actual reaction T for LOHC processes, the measurement results for λ_c are valuable to develop structure-property relationships and can also be used to test the aforementioned empirical prediction method for λ_c that is applicable up to elevated process-relevant T. For this purpose, but also for the evaluation and interpretation of the experimental results for λ_c, additional T-dependent measurements of the refractive index and infrared spectra of the same systems as investigated regarding λ_c, and measurements of the density of the three oxo-H0-BT regioisomers and all binary mixtures were also carried out in this work.

2. Experimental section

2.1. Materials and sample preparation

Table 1 lists the relevant information about the nine LOHC substances used in this study. The three regioisomers of H0-BT, i.e. H0-o-BT, H0-m-BT, and H0-p-BT, as well as those of H12-BT, i.e. H12-o-BT, H12-m-BT, and H12-p-BT, were taken from the same batches as the samples investigated by Kerscher et al. [16] with respect to their density, viscosity, and interfacial tension. In this study, details about the synthesis route for the six regioisomer samples and their analysis performed at the Helmholtz-Institut Erlangen-Nürnberg for Renewable Energies (HI ERN) can also be found [16]. The three regioisomers of oxo-H0-BT, i.e. oxo-H0-o-BT, oxo-H0-m-BT, and oxo-H0-p-BT, were obtained from commercial suppliers and were used as provided. For all regioisomers, the purity is provided by the supplier based on the peak area determined by gas chromatography (GC) and is specified to be 0.979 and larger. The

Table 1
Specification of the investigated chemicals.

Substance	CAS number	Chemical structure	Supplier	Molar mass $M/(g \cdot mol^{-1})$	Share of *cis* isomer	Purity
H0-o-BT	713-36-0	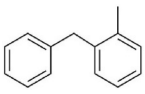	HI ERN	182.26	–	$w = 0.980$[a]
H0-m-BT	620-47-3	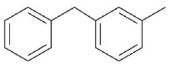	HI ERN	182.26	–	$w = 0.989$[a]
H0-p-BT	620-83-7	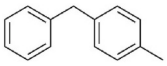	HI ERN	182.26	–	$w = 0.979$[a]
H12-o-BT	*cis*: 54,824-04-3 *trans*: 54.823-94-8	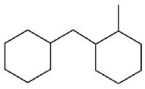	HI ERN	194.36	0.3621	$w = 0.985$[a]
H12-m-BT	*cis*: 54,823-96-0 *trans*: 54,823-95-9	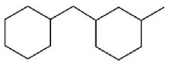	HI ERN	194.36	0.7404	$w = 0.985$[a]
H12-p-BT	*cis*: 54,823-97-1 *trans*: 54,823-98-2	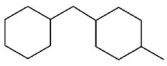	HI ERN	194.36	0.3752	$w = 0.979$[a]
oxo-H0-o-BT	131-58-8	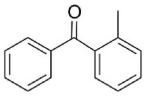	abcr GmbH	196.24	–	0.980 (by area)[b]
oxo-H0-m-BT	643-65-2	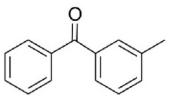	ThermoFisher Scientific	196.24	–	0.980 (by area)[b]
oxo-H0-p-BT	134-84-9	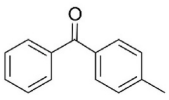	Apollo Scientific	196.24	–	0.990 (by area)[b]

[a] Purity as specified by GC coupled with coupled flame-ionization detection (FID).
[b] Purity as specified by supplier by GC.

small amount of impurities present in the samples is supposed to result in a negligibly small effect on the measurement results for λ_c because these impurities with a very small proportion are typically very similar to the substances of interest with comparable thermal conductivities. It should be mentioned that the H12-BT regioisomers show additionally stereoisomerism in the form of *cis* and *trans* stereoisomers. The relative share of the *cis* stereoisomer in the mixtures in terms of the amount fraction or mole fraction is also provided in Table 1 according to Ref. [16].

Based on the pure regioisomers, selected binary mixtures of H0-BT/H12-BT and H0-BT/oxo-H0-BT were prepared. In these mixtures, both components feature always the same type of regioisomerism based on the ortho- or para-isomers since the latter two types are typically predominantly found in the commercially available isomeric mixture of H0-BT [16]. The mixtures were prepared by using a balance (Sartorius Entris 224i-1S) with an expanded ($k = 2$) uncertainty of 1 mg. The mixing process involved at least five individual weighing steps of the samples. The five mixture samples with corresponding abbreviated names and the amount fractions of substance 1, x_1, and substance 2, $x_2 = 1 - x_1$, are listed in Table 2. For x_1 and x_2, the expanded ($k = 2$) uncertainty can be estimated to be 0.001, neglecting the influence of impurities.

Before the filling of the samples into the GPPI, they were sonicated over 15 min to ensure that no air bubbles are dissolved in the liquid phase. Based on the investigations of Berger Bioucas et al. [15], the sonication process has shown to have no influence on the characteristics of LOHC samples.

Table 2
Specification of the investigated binary mixtures.

Mixture name	Substance 1	Substance 2	x_1	x_2
o-BT-50	H0-o-BT	H12-o-BT	0.500[a]	0.500[a]
p-BT-25	H0-p-BT	H12-p-BT	0.749[a]	0.251[a]
p-BT-50	H0-p-BT	H12-p-BT	0.500[a]	0.500[a]
p-BT-75	H0-p-BT	H12-p-BT	0.250[a]	0.750[a]
o-BT/oxo-BT	H0-o-BT	oxo-H0-o-BT	0.483[a]	0.517[a]

[a] Amount fractions x_i were calculated based on M of the pure substances neglecting impurities. Expanded ($k = 2$) uncertainty of x_i is estimated to be 0.001.

2.2. Thermal conductivity by guarded parallel-plate instrument (GPPI)

The thermal conductivity λ_c of the samples listed in Table 1 and Table 2 was determined by a guarded parallel-plate instrument (GPPI) in the T range between (278.15 and 358.15) K in steps of 10 K at atmospheric pressure. The apparatus enables an absolute determination of λ_c without any calibration procedure. A detailed description of the apparatus and its measurement instrumentation and automation can be found in a previous study [23]. A former version of a GPPI was used for the investigation of λ_c of commercially available technical mixtures of H0-BT and H12-BT as well as similar LOHC substances in the form of

H0-DPM, H0-DBT, and their related hydrogenated forms [15]. In the following, the main principles of the method and experimental details relevant to this study are given.

The working principle of the GPPI is based on the one-dimensional form of the Fourier's Law of heat conduction for a planar plate according to the equation

$$\dot{Q}_{cond} = A\frac{\lambda_c}{s}(T_{hot} - T_{cold}) . \quad (1)$$

In Eq. (1), $\dot{Q}_{cond}$ is the purely conduction-related heat flow guided through the sample of heating transfer area A and thickness s as the result of a driving T difference between the outer surfaces of the sample, $\Delta T = (T_{hot} - T_{cold})$. Here, T_{hot} and T_{cold} refer to the temperatures at the surfaces of the upper heating plate and the lower cooling plate which are in contact with the sample of interest. The measured heat flow $\dot{Q}_{exp}$ may contain besides $\dot{Q}_{cond}$ also further superimposed heat flow contributions which need to be minimized or considered, which is briefly explained in the following.

The sample is placed perpendicularly to the gravitational field within the sample layer of the GPPI. Since T of the heating plate is larger than that of the cooling plate, i.e. the sample is heated from the top, it is ensured that heat flow contributions caused by advection inside the sample layer including Rayleigh-Bénard advection are eliminated [15, 23]. Furthermore, the thermal guard system around the heating plate suppresses the contribution of possible heat leakage flows between this plate and the surrounding to a minimum, as detailed in Ref. [23]. At last, a heat flow through the sample due to thermal radiation may be present and needs to be considered depending on the characteristics of the sample. To minimize radiation between the heating and cooling plates as much as possible, the surfaces in contact with the sample are covered with a thin layer of chrome with very low emission coefficient of around 0.04. Moreover, all samples used in this study can be considered as systems which partially absorb radiation. The radiation contribution λ_r can be approximated by the method suggested by Braun [39] and further developed by Poltz [40] and Kohler [41]. The obtained value for λ_r is then subtracted from the experimentally measured, effective thermal conductivity λ_{exp} ($=\lambda_c + \lambda_r$) to determine λ_c. The estimation method for λ_r requires information of the transmission spectra and the refractive index of the samples in the infrared wavelength range. The spectra for the transmission D were obtained at atmospheric p and T by a FT/IR-4100 Infrared Spectrometer from JASCO company at wavenumbers ν from (450–4500) cm^{-1} with an uncertainty $U(\nu) = 0.01$ cm^{-1} using a sample layer thickness s_0 of 1 μm. For all samples excluding oxo-H0-p-BT with a melting point at around 328 K, the measured transmission spectra are given in Figs. S1 and S2 in the Supporting Information. As the access to the refractive index in the infrared wavelength range is challenging, the refractive index at the sodium vapor line was measured with an Abbe refractometer, as described in section 2.3, and used as an approximation. For all studied samples, the estimated radiation contribution λ_r to λ_{exp} is between (1.0 and 3.0) % for the T range from (278.15–358.15) K.

In the GPPI, all relevant elements including the heating plate, cooling plate, and guard parts are made of copper with high thermal conductivity and are equipped with several Pt-100 Ω resistance probes for T measurement and control. The absolute uncertainty ($k = 2$) of each of these probes is $U(T) = 0.003$ K. All parts are heated independently using resistance heating. In the case of the heating plate, the electrical power supplied to the heating wire that is in direct contact with this plate is determined by measuring the voltage and electrical current via a DC power supply. This power corresponds to the value for $\dot{Q}_{exp}$. The sample thickness was adjusted to be $s = (1.961 \pm 0.020)$ mm ($k = 2$) and was kept constant for all measurements. The T differences between heating and cooling plate were varied at three values ΔT of (3.0, 3.5, and 4.0) K after reaching steady state. This leads to three separate measurement values for λ_c at every single mean $T = (T_{hot} + T_{cold})/2$, which were calculated from the average of 25 individual measurement points for each ΔT. The three individual values for λ_c values for each ΔT were then averaged to obtain the final measurement results for λ_c at each investigated T.

Before and after the investigations of the LOHC samples as well as between these studies, test measurements on λ_c were performed with deionized water at T of (303.15 and 293.15) K. In all cases, the experimental results for λ_c agree with reference data [42] recommended in the REFPROP database [43] clearly within combined uncertainties. In addition, a repetition measurement for at least one pure regioisomer of each system class was performed at T = (303.15 or 313.15) K after investigating the largest T. Again, the λ_c data from the repetition were found to agree with the initial measurement within combined expanded uncertainties. This indicates a thermal stability of all studied samples within the measurement series. The uncertainties of the experimentally determined values for λ_c was calculated according to Gaussian error propagation calculations as described in Ref. [23]. Here, the individual uncertainties of the input parameters entering the working equation, Eq. (1), are considered. Among the individual contributions to the uncertainty of λ_c, the ones associated with s and T are the most influencing parameters. The relative expanded ($k = 2$) uncertainty $U_r(\lambda_c)$ ranges between 0.019 and 0.021 and shows an average value of 0.020.

2.3. Refractive index by Abbe refractometer

The refractive index n_D at the sodium vapor line ($\lambda_D = 589.3$ nm) and the refractive index difference $n_F - n_C$ for the Fraunhofer lines F ($\lambda_F =$ 486.1 nm) and C ($\lambda_C = 656.3$ nm) of the pure regioisomers and the binary mixtures were measured with an Abbe refractometer (type AR4, Krüss GmbH). All measurements were carried out at atmospheric p of 0.1 MPa in the T range from (278.15–358.15) K in steps of 10 K. Only for oxo-H0-p-BT, the lowest T was set to 328.15 K due to its melting point. By using a thermostatic bath, T of the sample was controlled which was measured with an integrated T sensor with an expanded ($k = 2$) uncertainty of 1 K. The expanded ($k = 2$) uncertainties are estimated to be 0.0005 for n_D and 0.001 for $n_F - n_C$.

2.4. Density – vibrating U-tube densimeter

The supplemental measurements of liquid density ρ of the three regioisomers of oxo-H0-BT and of the binary mixtures were performed with a vibrating U-tube densimeter (type DMA 5000, Anton Paar GmbH). All measurements were performed under atmospheric p of 0.1 MPa in the T range from (278.15–358.15) K in steps of 10 K. This was also possible for oxo-H0-p-BT which could be subcooled below its melting point. The relative expanded ($k = 2$) uncertainty of the measured ρ can be stated to be $U_r(\rho) = 2{\cdot}10^{-4}$ and an expanded ($k = 2$) absolute uncertainty of the temperature of $U(T) = 0.01$ K.

3. Results and discussion

This section discusses firstly the measurement results for the refractive index and density, which are also helpful for the analysis of structure-property relationships. Afterwards, the focus is on the thermal conductivity of the LOHC samples. Here, the T-dependent measurement results of the pure regioisomers of H0-BT, H12-BT, and oxo-H0-BT as well as of the relevant binary mixtures will be presented and analyzed. In the last part, the experimental data for λ_c of the pure regioisomers will be used to test an available prediction model for the thermal conductivity of cyclic hydrocarbons.

3.1. Refractive index

For all pure and binary systems studied in this work, the measurement data for n_D and the difference $n_F - n_C$ can be found in Table S1 of the Supporting Information. The T-dependent measurement data for n_D

of the pure regioisomers can be represented by an unweighted linear fit according to

$$n_{calc} = n_0 + n_1 T. \quad (3)$$

The corresponding fit parameters n_0 and n_1 and the average absolute relative deviation (AARD) of the experimental data from the fit are listed in Table 3. In all cases, the deviations of the experimental data for n_D from n_{calc} are smaller than the measurement uncertainty.

For the pure regioisomers as well as the studied binary mixtures, further experimental data for n_D are not available in the literature to the best of the authors' knowledge. Only for the technical mixtures of regioisomers of H0-BT and H12-BT, n_D data are reported by Rüde et al. [44] and Berger Bioucas et al. [15]. In both of these studies, however, no information about the contents of the individual isomeric compounds in the H0-BT and H12-BT samples could be specified. Since the study of Rüde et al. [44] provides no clear specification of T, a data comparison is not possible. The experimental n_D values provided by Berger Bioucas et al. [15] for the technical mixtures of H0-BT and H12-BT from (298.15–323.15) K agree within combined uncertainties with the corresponding n_{calc} data of either dehydrogenated and hydrogenated regioisomers obtained in this work. This behavior is a result of the very small variations in n_D as a function of the regioisomerism, as discussed below.

In general, n_D decreases with increasing T, which is commonly observed for organic liquids. Considering the values for n_1 in Table 3, this T-dependent decrease is very similar between the different regioisomers for each class. Among the three different fluid classes, the partially oxidized oxo-H0-BT components show the largest n_D values, followed by the dehydrogenated H0-BT components and then by the hydrogenated H12-BT components. This order corresponds to the order in ρ. Comparing the values for the different isomers, all regioisomers can be clearly distinguished from one another, however, H0-o-BT shows distinctly higher values by 0.005–0.006 than the other two regioisomers. The same statement is also true for the three corresponding H12-BT isomers, where H12-o-BT shows values larger by around 0.004 than the other regioisomers. For the oxo-H0-o-BT and oxo-H0-m-BT regioisomers, the data for n_D agree with each within combined uncertainties, where oxo-H0-p-BT has distinctly the largest values. For the binary mixtures H0-p-BT/H12-p-BT and H0-o-BT/oxo-H0-o-BT, the experimental n_D data show negative deviations from a linear amount fraction-based mixing rule at all T studied. This behavior was also observed by Berger Bioucas et al. [15] for mixtures consisting of the technical mixtures of H0-BT and H12-BT as well as for mixtures of H0-DPM and H12-DPM, and also for binary mixtures of other structurally similar substances like the pair benzene/cyclohexane [45].

3.2. Density

The experimental data for ρ of the three regioisomers of oxo-H0-BT and the binary mixtures listed in Table 2 can be found in Table S2 of the Supporting Information. For the pure regioisomers of H0-BT and H12-BT, the corresponding results for ρ were already presented and discussed in a previous study [16]. Based on the samples used in this study, the corresponding binary mixtures H0-BT/H12-BT and H0-BT/oxo-H0-BT were prepared. The experimental data for ρ of the pure regioisomers oxo-H0-o-BT, oxo-H0-p-BT, and oxo-H0-p-BT were correlated as a function of T by a polynomial of second order according to

$$\rho_{calc}(T) = \rho_0 + \rho_1 T + \rho_2 T^2, \quad (4)$$

with all data points having the same statistical weight in the fitting procedure. For the fitting here and in all other cases, nonlinear regressions are performed based a Levenberg–Marquardt algorithm, where the sum of the squares of the deviations between the experimental and fitted values is minimized. The corresponding fit parameters are listed with the AARD values in Table 4.

3.2.1. Pure regioisomers of oxo-H0-BT

The upper part of Fig. 1 shows the experimental ρ and ρ_{calc} of the three regioisomers of oxo-H0-BT as a function of T, while the lower part illustrates the relative deviations of these data from the fit correlation Eq. (4) connected to oxo-H0-p-BT, $\rho_{calc,oxo\text{-}H0\text{-}p\text{-}BT}$. The correlations describe the measurement data well within their uncertainty, as can be seen from the lower part of Fig. 1. To the best of the authors' knowledge, there are no further experimental data available in the literature for ρ of the pure regioisomers of oxo-H0-BT.

According to Fig. 1, ρ shows the typical behavior of organic liquids with decreasing values for increasing T. A larger T corresponds to higher thermal energies and weaker intermolecular forces [46,47], which is related to larger mean distances between molecules and smaller ρ. The T-dependent decrease of ρ is very similar for all three isomers, resulting in relative changes of (−5.67 to −5.78) % from (278.15–358.15) K. Here, oxo-H0-p-BT exhibits the least pronounced T-dependency. Comparing ρ of the three regioisomers, significant relative differences between the measurement values can be found, which are mostly larger than the combined uncertainties. Only at T = (278.15 and 288.15) K, the relative deviations between ρ of oxo-H0-o-BT and oxo-H0-p-BT are within combined uncertainties, i.e. within 0.04 %. In accordance with the behavior of n_D, the ρ values of the three oxo-H0-BT regioisomers are larger than those of the H0-BT regioisomers [16], which are larger than those of the H12-BT regioisomers [16]. This indicates that the increasing polar character including polarizability from H12-BT over H0-BT to oxo-H0-BT results in stronger attractive intermolecular forces and, thus larger ρ values. For example, the increase of ρ from H0-o-BT to oxo-H0-o-BT is relatively large with 8.3 % at 308 K, although M and the size of the two molecules are quite similar. Thus, the behavior of ρ seems to be mainly caused by the fact that the carbonyl group is very polar with a strongly electronegative oxygen atom and electropositive carbon. As Mahl et al. [48] have discussed for the analog toluene/benzaldehyde pair, induced dipole-dipole interactions between the carbonyl group and the phenyl ring can be formed, which macroscopically lead to the relatively high ρ values for oxo-H0-BT. While oxo-H0-o-BT shows the smallest ρ among the oxygenated regioisomers, the ortho-based isomers H0-o-BT and H12-o-BT have shown the largest ρ among the dehydrogenated and hydrogenated regioisomers [16]. For the latter two classes, Kerscher et al. [16] have argued that the closer proximity between the methyl group in the phenyl ring and the methylene group in H0-o-BT may result in an overall sterically denser packing. In the case of the oxo-H0-BT isomers, it seems that the interplay between the relatively polar carbonyl group and the non-polar methyl groups seems to be responsible for the different behavior found among the oxygenated regioisomers.

Interestingly, oxo-H0-p-BT could be investigated in a liquid state down to 278.15 K below its melting point of around 328 K. Such supercooled metastable behavior was already reported for the partially oxygenated form of H0-DPM given by benzophenone (oxo-H0-DPM)

Table 3
Coefficients of Eq. (3) for the calculation of the refractive index n_{calc} of the studied pure regioisomers.

Sample	n_0	n_1/K^{-1}	T/K	AARD[a] / %
H0-o-BT	1.7226	$-5.02\cdot10^{-4}$	278.15–358.15	0.022
H0-m-BT	1.7174	$-5.02\cdot10^{-4}$	278.15–358.15	0.020
H0-p-BT	1.7163	$-5.03\cdot10^{-4}$	278.15–358.15	0.021
H12-o-BT	1.6051	$-4.35\cdot10^{-4}$	278.15–358.15	0.011
H12-m-BT	1.6051	$-4.46\cdot10^{-4}$	278.15–358.15	0.058
H12-p-BT	1.6004	$-4.35\cdot10^{-4}$	278.15–358.15	0.016
oxo-H0-o-BT	1.7452	$-4.97\cdot10^{-4}$	278.15–358.15	0.029
oxo-H0-m-BT	1.7400	$-4.81\cdot10^{-4}$	278.15–358.15	0.032
oxo-H0-p-BT	1.7534	$-5.10\cdot10^{-4}$	278.15–358.15	0.009

[a] Average absolute relative deviation of the measurement data from the fit.

Table 4
Coefficients of Eq. (4) for the liquid density ρ_{calc} of the studied regioisomers of oxo-H0-BT.

Sample	ρ_0/(kg·m^{-3})	ρ_1/(kg·m^{-3}·K^{-1})	ρ_2/(kg·m^{-3}·K^{-2})	T range/K	AARD[a]/%
oxo-H0-o-BT	$1.32128 \cdot 10^3$	$-8.21532 \cdot 10^{-1}$	$4.63527 \cdot 10^{-5}$	278.15–358.15	$5.78 \cdot 10^{-4}$
oxo-H0-m-BT	$1.31527 \cdot 10^3$	$-7.74601 \cdot 10^{-1}$	$-1.42121 \cdot 10^{-5}$	278.15–358.15	$8.65 \cdot 10^{-4}$
oxo-H0-p-BT	$1.31335 \cdot 10^3$	$-7.83156 \cdot 10^{-1}$	$1.41242 \cdot 10^{-5}$	278.15–358.15	$5.51 \cdot 10^{-4}$

[a] Average absolute relative deviation of the measurement data from the fit.

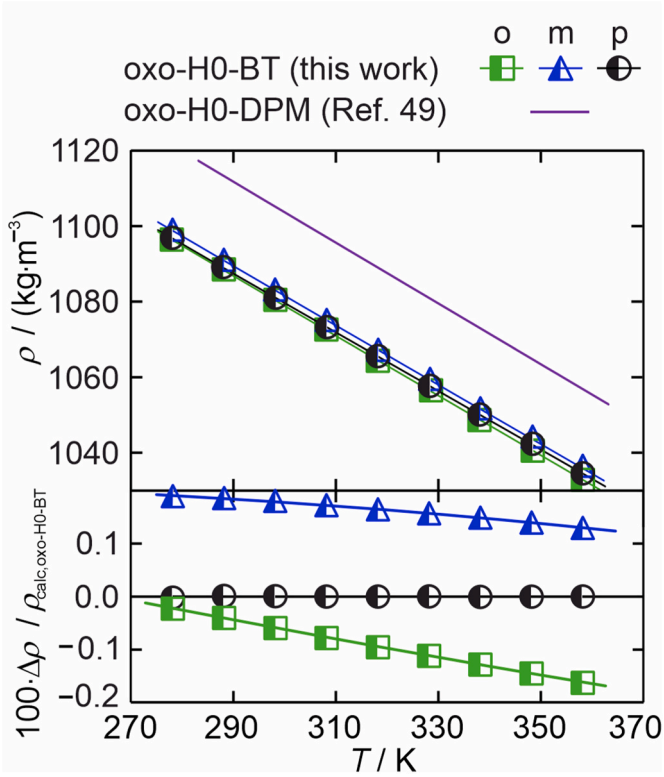

Fig. 1. Upper part: Experimental liquid density data for the three oxo-H0-BT regioisomers as a function of T at ambient pressure including the corresponding fit ρ_{calc} based on Eq. (4) and the analog fit for oxo-H0-DPM reported by Kerscher et al. [49]. Lower part: Relative deviations of the experimental ρ data and ρ_{calc} of the three oxo-H0-BT regioisomers from $\rho_{calc,oxo\text{-}H0\text{-}p\text{-}BT}$.

[49–52], which has a structure very similar to oxo-H0-BT and includes also a carbonyl group. As can be seen in the upper part of Fig. 1, ρ of oxo-H0-DPM reported by Kerscher et al. [49] is distinctly larger than that of any regioisomer of oxo-H0-BT. It seems that the addition of a methyl group causes a less pronounced packing of the oxo-H0-BT regioisomers compared to that of oxo-H0-DPM.

3.2.2. *Binary mixtures of H0-BT/H12-BT and H0-BT/oxo-H0-BT*

The experimental data for density of the binary mixtures indicated by ρ_{mix} can be discussed as a function of composition in terms of the amount fraction x_i with the help of simple mixing rule via

$$\rho_{mix} = \frac{\sum_i x_i M_i}{V_m^E + \sum_i \frac{x_i M_i}{\rho_i}}. \quad (5)$$

Here, M_i is the molar mass of the two mixture components i. In Eq. (5), the parameter V_m^E is the so-called excess molar volume and reflects the difference between the real and the ideal molar volume of the mixture.

First, the binary mixtures involving H0-BT and H12-BT regioisomers are analyzed, which are given by the para-based mixtures H0-p-BT/H12-p-BT. By applying Eq. (5) with $V_m^E = 0$, the resulting AARDs of the correlated ρ_{mix} data from the T-dependent experimental results are (0.35, 0.45, 0.32) % for the 25-p-BT, 50-p-BT and 75-p-BT mixtures, respectively, which are distinctly larger than the measurement uncertainty of 0.02 %. Moreover, all of the calculated excess molar volumes are positive, indicating that intermolecular forces between molecules of different species seem to be weaker than between like molecules. Fig. 2 shows the values for V_m^E calculated from Eq. (5) as a function of the amount fraction of the hydrogenated species x_{H12} at selected T. In addition to the present results for the H0-p-BT/H12-p-BT mixtures, the results for the H0-o-BT/H12-o-BT and H0-DPM/H12-DPM mixtures reported by Kerscher et al. [16] and Schmidt et al. [53] are given. Within the studied T, V_m^E is almost T-independent for all systems, which has also been observed for other binary mixtures of a dehydrogenated and hydrogenated component [16,53,54]. Furthermore, the V_m^E values are positive in all cases, which indicates that attractive intermolecular forces between molecules of different species seem to be weaker than between like molecules. While the H0-based components show a certain polar character due to their aromatic rings which allow for π-π-stacking and edge-to-face interactions [55], the H12-based components are rather non-polar and, thus, do not preferentially interact with H0-based components. The largest values for V_m^E can be found for equimolar mixtures with $x_{H12} = 0.50$, where the statistical probability of interactions between molecules of different species is *per se* the highest.

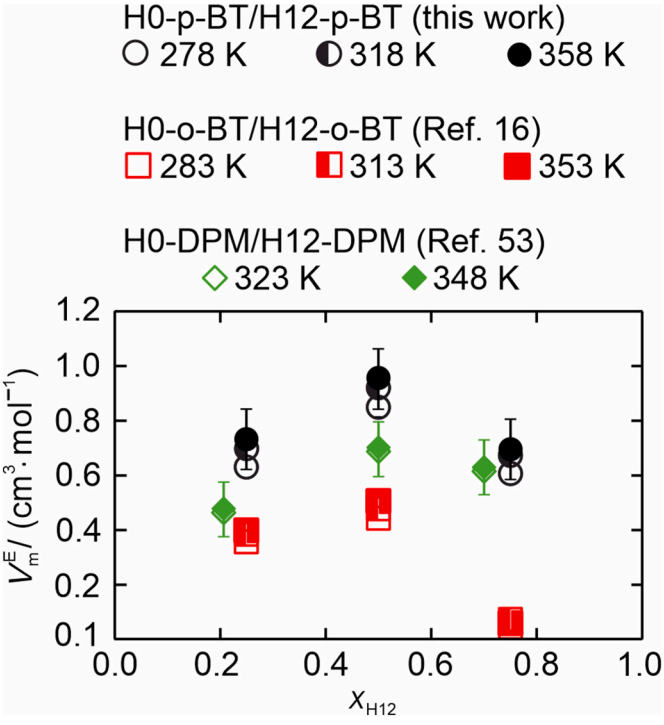

Fig. 2. Excess molar volume of binary mixtures of H0-p-BT and H12-p-BT as a function of the amount fraction x_{H12} of the hydrogenated component at selected T calculated based on Eq. (5) using the present measurement results for ρ. For comparison, the V_m^E data for the binary mixtures of H0-o-BT and H12-o-BT from Kerscher et al. [16] and for those of H0-DPM and H12-DPM from Schmidt et al. [53] were added.

Comparing the different mixture types with each other, the H0-p-BT/H12-p-BT mixtures show the largest magnitude for V_m^E that is about twice as large as for H0-o-BT/H12-o-BT [16]. Reasons for this behavior are speculative, yet may be related to the more pronounced sterical bulkiness of the p-based regioisomers compared to the o-based ones. Interestingly, the V_m^E data for the H0-DPM/H12-DPM mixtures [53], which do not contain the methyl group in the phenyl and cyclohexyl rings, are very close to those for the H0-p-BT/H12-p-BT mixtures.

In addition, the binary mixture of the dehydrogenated H0-o-BT and the partially oxidized oxo-H0-o-BT was investigated with respect to ρ at one representative amount fraction of $x_{oxo} = 0.517$ for oxo-H0-o-BT. Using Eq. (5) under the assumption of $V_m^E = 0$, the calculated ρ_{mix} data deviate by less than 0.06 % from the experimental data for all the studied T from (278.15–358.15) K, which is outside the experimental uncertainty. Additionally, the literature data for binary mixture of diphenylmethane and benzophenone from Kerscher et al. [49] was added for comparison. In all cases, V_m^E of the binary H0-o-BT/oxo-H0-o-BT mixture is negative with values ranging from (−0.13 to −0.09) $cm^3 \cdot mol^{-1}$ at T = (278.15–358.15) K. While V_m^E is again practically independent of T within expanded uncertainties, the sign of V_m^E is different from that discussed for the binary mixtures H0-BT/H12-BT in Fig. 2, although the absolute magnitude is around one order of magnitude smaller. Nevertheless, negative V_m^E values indicate that the unlike molecules interact more strongly with each other than like molecules, which may originate from induced dipole-dipole interactions between the aromatic ring of the H0-BT and the carbonyl group of the oxo-H0-BT molecules [48]. Negative V_m^E were also reported by Kerscher et al. [49] for similar binary mixtures consisting of H0-DPM and oxo-H0-DPM, although the absolute magnitude was larger for the latter mixtures.

3.3. Thermal conductivity

3.3.1. Summary of experimental results

For the thermal conductivity λ_c as central property of interest in this study, the measurement results obtained by the GPPI are summarized in Table 5. For the nine pure regioisomers and five binary mixtures, the measurements were performed at atmospheric pressure at T from (278.15–358.15) K. Only for oxo-H0-p-BT, the lowest T was limited to 328.15 K due to its melting point.

3.3.2. Pure regioisomers

For each pure regioisomer, the measurement results for λ_c listed in Table 5 could be represented well by a polynomial fit of second order as a function of T according to

$$\lambda_{c,calc}(T) = \lambda_0 + \lambda_1 T + \lambda_2 T^2, \quad (6)$$

with all single data points having the same stasistical weight. For oxo-H0-p-BT, where only a limited T range could be studied, a linear fit with $\lambda_2 = 0$ was sufficient. The corresponding fit parameters λ_0, λ_1, and λ_2 as well as the respective AARD of the calculated $\lambda_{c,calc}$ data from the measurement data are listed in Table 6. It should be noted that the parameters in Table 6 are only valid within the specified T range of the measurements for improved data representation and should be used outside this range for extrapolations with caution. Although a linear T-dependent fit of the measured λ_c data gives a larger AARD than Eq. (6), the former is considered to provide a better extrapolative character for large T up to regions relevant for hydrogenation and dehydrogenation processes. Such linear behavior of λ_c as a function of T is commonly observed for organic liquids sufficiently far away from the critical point. Based on a linear unweighted fit of the measurement data for λ_c as a function of T in Table 5, the extrapolated values for λ_c of the ortho-based BT-compounds H0-o-BT, H12-o-BT, and oxo-H0-o-BT as example substances were calculated at T of 523.15 K, which is representative for the lower T window of the dehydrogenation and partial oxidation steps. The corresponding values are (0.090, 0.090, and 0.095) $W \cdot m^{-1} \cdot K^{-1}$ for H0-o-BT, H12-o-BT, and oxo-H0-o-BT, i.e. close to values of (0.09–0.10) $W \cdot m^{-1} \cdot K^{-1}$, which is also valid for all other substances at 523.15 K.

Fig. 3 shows the experimental data for λ_c of the ortho-, meta-, and para-based pure regioisomers of H0-BT, H12-BT, and oxo-H0-BT determined in this work as a function of T. The upper part provides the absolute values, while the lower part gives the relative deviations of the measured λ_c from the fit $\lambda_{c,calc}$ based on Eq. (6) for each regioisomer. Due to legibility reasons, the error bars representing the expanded ($k = 2$) uncertainty of 2 % were added in the upper part only to the markers for (278.15 and 358.15) K. As can be seen in Fig. 3 and from Table 6, $\lambda_{c,calc}$ describes the experimental data well within their uncertainties. All measured values for λ_c of the H0-BT, H12-BT, and oxo-H0-BT regioisomers are in the range of (0.10–0.13) $W \cdot m^{-1} \cdot K^{-1}$, which is within the typically expected range for organic substances of about (0.1–0.2) $W \cdot m^{-1} \cdot K^{-1}$ [31]. Moreover, the commonly observed trend of decreasing λ_c with increasing T is observed. Among the three classes, λ_c of the H0-BT regioisomers shows the steepest decrease from

Table 5
Measurement results for the thermal conductivity λ_c of the investigated pure and binary LOHC systems obtained by the GPPI at atmospheric pressure p for various temperatures T.[a]

	λ_c/(W·m^{-1}·K^{-1})								
T/K	278.15	288.15	298.15	308.15	318.15	328.15	338.15	348.15	358.15
pure regioisomers									
H0-o-BT	0.1271	0.1250	0.1249	0.1235	0.1218	0.1204	0.1187	0.1171	0.1138
H0-m-BT	0.1298	0.1278	0.1274	0.1254	0.1235	0.1214	0.1189	0.1160	0.1133
H0-p-BT	0.1301	0.1277	0.1274	0.1265	0.1245	0.1225	0.1202	0.1174	0.1134
H12-o-BT	0.1091	0.1080	0.1070	0.1063	0.1056	0.1050	0.1044	0.1039	0.1023
H12-m-BT	0.1077	0.1071	0.1062	0.1058	0.1051	0.1046	0.1039	0.1032	0.1012
H12-p-BT	0.1087	0.1075	0.1069	0.1064	0.1052	0.1046	0.1039	0.1031	0.1010
oxo-H0-o-BT	0.1285	0.1269	0.1257	0.1244	0.1228	0.1214	0.1198	0.1202	0.1169
oxo-H0-m-BT	0.1290	0.1270	0.1266	0.1258	0.1245	0.1236	0.1227	0.1214	0.1184
oxo-H0-p-BT	–	–	–	–	–	0.1267	0.1230	0.1222	0.1207
binary mixtures									
p-BT-25 ($x_{H12\text{-}p\text{-}BT} = 0.251$)	0.1212	0.1203	0.1194	0.1185	0.1164	0.1155	0.1145	0.1134	0.1096
p-BT-50 ($x_{H12\text{-}p\text{-}BT} = 0.500$)	0.1158	0.1154	0.1140	0.1126	0.1114	0.1102	0.1088	0.1077	0.1052
p-BT-75 ($x_{H12\text{-}p\text{-}BT} = 0.750$)	0.1121	0.1099	0.1089	0.1080	0.1066	0.1054	0.1043	0.1031	0.1010
o-BT-50 ($x_{H12\text{-}o\text{-}BT} = 0.500$)	0.1134	0.1138	0.1127	0.1118	0.1107	0.1096	0.1086	0.1077	0.1055
o-BT/oxo-BT ($x_{H0\text{-}o\text{-}BT} = 0.483$)	0.1256	0.1250	0.1237	0.1233	0.1218	0.1213	0.1208	0.1205	0.1183

[a] The expanded uncertainties ($k = 2$) for T, p, and x are $U(T) = 0.01$ K, $U(p) = 3$ kPa, and $U(x) = 0.001$. The relative expanded uncertainty ($k = 2$) for λ_c is $U_r(\lambda_c) = 0.02$.

Table 6
Coefficients of Eq. (6) for the thermal conductivity $\lambda_{c,calc}$ of the studied pure LOHCs.

Sample	λ_0/(W·m^{-1}·K^{-1})	λ_1/(W·m^{-1}·K^{-2})	λ_2/(W·m^{-1}·K^{-3})	T range/K	AARD[a]/%
H0-o-BT	$7.256\cdot10^{-2}$	$4.652\cdot10^{-4}$	$-9.737\cdot10^{-7}$	278.15–358.15	0.27
H0-m-BT	$5.569\cdot10^{-2}$	$6.304\cdot10^{-4}$	$-1.312\cdot10^{-6}$	278.15–358.15	0.14
H0-p-BT	$4.213\cdot10^{-4}$	$9.737\cdot10^{-4}$	$-1.834\cdot10^{-6}$	278.15–358.15	0.32
H12-o-BT	$1.403\cdot10^{-1}$	$-1.411\cdot10^{-4}$	$1.016\cdot10^{-7}$	278.15–358.15	0.21
H12-m-BT	$8.714\cdot10^{-2}$	$1.864\cdot10^{-4}$	$-4.069\cdot10^{-7}$	278.15–358.15	0.25
H12-p-BT	$1.009\cdot10^{-1}$	$1.145\cdot10^{-4}$	$-3.150\cdot10^{-7}$	278.15–358.15	0.27
oxo-H0-o-BT	$1.690\cdot10^{-1}$	$-1.542\cdot10^{-4}$	$2.944\cdot10^{-8}$	278.15–358.15	0.27
oxo-H0-m-BT	$9.846\cdot10^{-2}$	$2.802\cdot10^{-4}$	$-6.212\cdot10^{-7}$	278.15–358.15	0.33
oxo-H0-p-BT	$1.879\cdot10^{-1}$	$-1.887\cdot10^{-4}$	–	328.15–358.15	0.45

[a] Average absolute relative deviation of the measurement data from the fit.

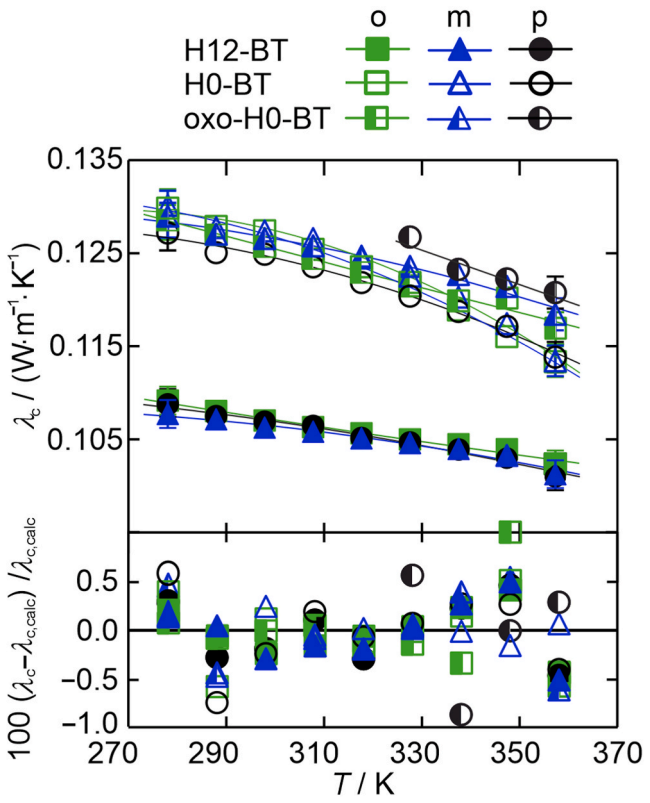

Fig. 3. Upper part: Experimental thermal conductivity λ_c of the regioisomers H0-(o, m, p)-BT, H12-(o, m, p)-BT, and oxo-H0-(o, m, p)-BT as a function of T at ambient pressure including the corresponding fits $\lambda_{c,calc}$ (lines) based on Eq. (6). Lower part: Relative deviations of the experimental λ_c data from the corresponding correlation $\lambda_{c,calc}$. Error bars indicating the expanded ($k = 2$) uncertainty of the experimental λ_c data are only shown for exemplary state points.

(278.15–358.15) K by (−10.5 to −12.9) %. The changes are smaller for the two oxidized regioisomers oxo-H0-m-BT and oxo-H0-o-BT with (−8.2 and −9.0) % and are least pronounced for the H12-BT regioisomers with values of (−6.1 to −7.1) %. In comparison with structurally similar substances, the experimental results for H0-DPM and H12-DPM obtained with the former GPPI [12] are 8.4 % and 4.2 % larger at 318.15 K than those for H0-o-BT and H12-o-BT, respectively. This shows that the addition of the methyl group from the DPM-to the BT-related components causes a pronounced decrease of λ_c, as it is also observed for the pairs benzene/toluene and cyclohexane/methylcyclohexane [43].

It can be seen from Fig. 3 that the dehydrogenated compounds H0-BT and its oxidized form oxo-H0-BT have similar λ_c values that are distinctly larger than those of the hydrogenated H12-BT counterparts. This finding can be discussed in terms of the molecular origin of thermal conduction. The thermal conductivity describes the transport of thermal energy between molecules in the absence of a macroscopic flow field [31]. In the case of liquids, this transport can be related to vibrational modes and translational modes. The vibrational modes are widely regarded to be much more important than the translational ones [31,56], especially at T near the freezing or melting point [57], which is valid for the substances examined in this work. The vibrational modes can be considered as oscillations around an equilibrium point or gravity center of the molecule [31,57] and resemble the energy phonons of a solid phase. The molecules in a liquid can move freely, but only within a certain frame. Such a so-called quasi-lattice frame [31,56,58] consists of the molecule in the center and all of its neighbors which constantly pull on each other and repel each other, depending on the distance between their atoms at the boundaries. In this concept, the density is an important macroscopic property since it indicates the mean intermolecular distances and the strength of the intermolecular forces. An increase in ρ is often related to increasing attractive intermolecular forces accompanied by decreasing mean intermolecular distances. This scenario is often associated with an increasing strength of vibrational modes and, thus, larger values for λ_c.

The measurement results for λ_c of the three studied LOHC classes follow the aforementioned conception qualitatively. By comparing the dehydrogenated and hydrogenated para-based compounds first, λ_c of H12-p-BT is 16.4 % smaller than that of H0-p-BT at $T = 278.15$ K. This decrease correlates well with the behavior of ρ, where H12-p-BT shows a 12.0 % lower density than H0-p-BT at the same T. Similar trends are also found for the dehydrogenated/hydrogenated pairs benzene/cyclohexane [59] or H0-DPM/H12-DPM [15]. The aromatic phenyl rings feature not only stronger electrostatic intermolecular forces than the rather non-polar cyclohexyl rings, but have also more compact flat shape. In contrast, the cyclohexyl rings take the so-called boat or chair shape [60,61], which appears to lead to larger mean distances between H12-BT molecules compared to H0-BT. As a result, the macroscopic properties ρ and λ_c are lower for H12-BT than for H0-BT.

The correlation between λ_c and ρ is less pronounced among the H0-BT and oxo-H0-BT classes. By partial oxidation of H0-o-BT to oxo-H0-o-BT, for example, λ_c increases only slightly by +1.1 % at 278.15 K, which is within the measurement uncertainty of 2 %. At the same T, ρ increases much more significantly by +9.8 % for oxo-H0-o-BT relative to H0-o-BT. At T above 348 K, the difference in λ_c between the ortho-based pair exceeds +2 %. Similar changes for λ_c and ρ can be seen for the meta-based regioisomer pairs. Only for the para-based pairs, the differences in λ_c between oxo-H0-p-BT and H0-p-BT are slightly larger with a maximal relative deviation of about 6.4 % at 358.15 K, which is better visible in the right part of Fig. 4. The small increase in the λ_c due to the partial oxidation from H0-BT to oxo-H0-BT could probably arise from the enhancing contribution of the highly polar carbonyl group to thermal conduction, through increase in polarizability. This carbonyl group of larger molecular weight than the methylene group causes also a strong increase in ρ, as described in chapter 3.2. It seems that the effect of this group on ρ is more pronounced than that on λ_c, which indicates that the strength of the vibrational modes on λ_c and the mean distance between the molecules are not much different for the H0-BT and oxo-H0-

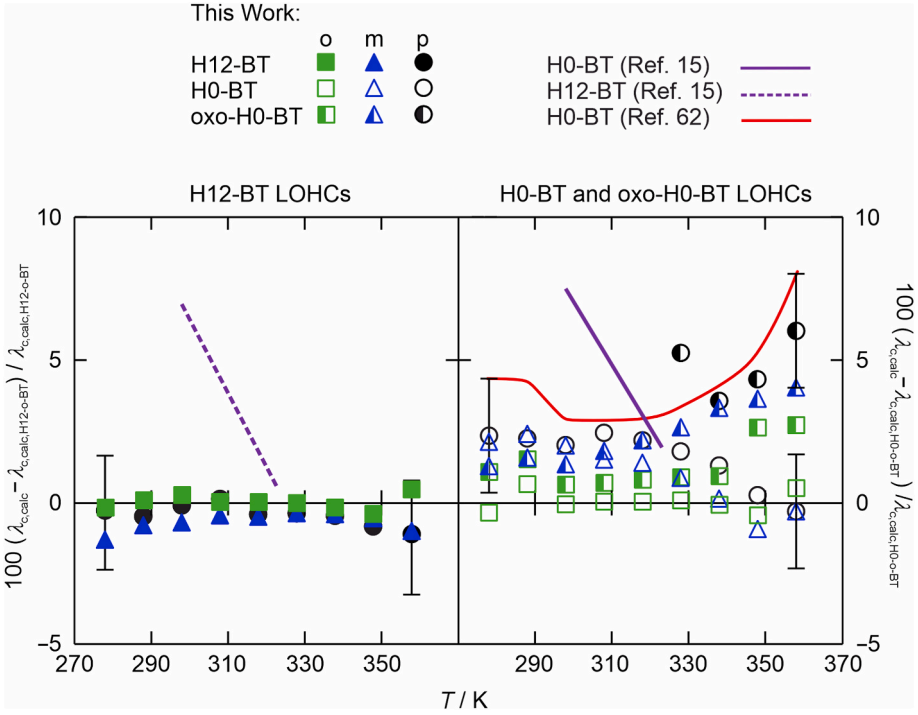

Fig. 4. Relative deviation of the present measurement results for λ_c of the hydrogenated H12-(o, m, p)-BT regioisomers from $\lambda_{c,calc}$ of H12-o-BT (left part) as well as those of the dehydrogenated H0-(o, m, p)-BT and partially oxidized oxo-H0-(o, m, p)-BT regioisomers from $\lambda_{c,calc}$ of H0-o-BT. In addition, the experimental λ_c data for the technical mixtures of H12-BT and H0-BT from Berger Bioucas et al. [15] as well as λ_c values for a technical mixture of H0-BT from Eastman Company [62] are added in the respective figure part. Error bars indicating the expanded ($k = 2$) uncertainty of the experimental λ_c data are only shown for exemplary state points.

BT regioisomers.

To resolve the differences between the different regioisomers of the three classes in more detail, Fig. 4 shows the relative deviations of the present measurement results for λ_c from $\lambda_{c,calc}$ of the ortho-based regioisomer as a reference. The left part focuses on the hydrogenated H12-BT systems, which includes the results for the technical H12-BT mixture measured by Berger Bioucas et al. [15]. In the right part of Fig. 4, the data for the dehydrogenated H0-BT and partially oxygenated oxo-H0-BT systems are shown. In addition to the λ_c data for the regioisomers from this study, also data for the technical H0-BT mixtures are given in the form of the measurement results reported by Berger Bioucas et al. [15] and values provided by Eastman Company [62]. Due to legibility reasons, only exemplary error bars indicating the expanded measurement uncertainties are drawn for the different data sets. As can be seen from Fig. 4, the regioisomerism has no significant impact on λ_c for each of the three classes of LOHC systems investigated in this study. The relative differences in λ_c between the o-, m-, and p-regioisomers of H0-BT, H12-BT, and oxo-H0-BT never exceed (2.5, 1.3, and 3.3) %, respectively, which corresponds to agreement within combined uncertainties in all cases and mostly within single uncertainties. Similarly small differences for λ_c were also reported in the literature [63] between the o-, m-, and p-regioisomers of xylene with a maximum relative deviation of 3 %. The largest relative differences between the λ_c data are observed for oxo-H0-BT regioisomers, where oxo-H0-p-BT has the largest values. Although being speculative, this behavior may be related to its special fluid character in the vicinity of the supercooled metastable region. Further experimental data for all the studied pure regioisomers are not available to the best of the authors' knowledge.

Considering the data for the technical mixtures of H12-BT and H0-BT from Berger Bioucas et al. [15], agreement with the present results within or at the edge of the combined uncertainties can be found. However, the T-dependent trend for λ_c of H12-BT and H0-BT reported by Berger Bioucas et al. [15] is much steeper compared to the data obtained for this work. This can be attributed to the fact that the former data were measured with an older version of the GPPI, which is described by Rausch et al. [64]. In this older version characterized with a larger uncertainty for λ_c of 5 %, heat leakage from the hot plate to the surrounding could not be fully suppressed, which resulted effectively in slightly too large results for λ_c, especially at low T. Moreover, the λ_c data for H0-BT provided by Eastman Company [62] as supplier of the commercially available H0-BT technical mixture are larger than the present measurement results, in particular at larger T. At $T = 358.15$ K, for example, the deviation of λ_c stated by Eastman Company relative to λ_c of H0-o-BT is +7.9 %. It has to be noted that neither the measurement method nor the uncertainty of λ_c is specified in the data sheet of the company.

3.3.3. *Binary mixtures of H0-BT/H12-BT and H0-BT/oxo-H0-BT*

Fig. 5 shows the experimental data for λ_c of the three investigated binary mixtures of H0-p-BT and H12-p-BT as a function of x_{H12} for three representative T of (278.15, 318.15, and 358.15) K. Here, also the measurement results for the pure substances H0-p-BT and H12-p-BT are included. The measurement data for λ_c of the binary mixture of H0-o-BT and H12-o-BT with $x_{H12} = 0.500$ is not shown in Fig. 5 due to legibility reasons. This ortho-based regioisomer pair shows the same kind of behavior as the para-based pair, which can be taken as representative for mixtures of dehydrogenated and hydrogenated BT-based mixtures.

All data sets for the binary mixtures presented in Fig. 5 show a similar mixture behavior, where λ_c of the mixtures is below the straight line connecting the data points of pure substances, which represents a simple linear amount fraction-based mixing rule. The largest deviations of the measured λ_c data from the linear mixing rule are −3.0 % at $T =$ 278.15 K and −1.9 % at $T = 278.15$ K for $x_{H12} = 0.5$, where also the largest V_m^E values were found according to section 3.2. The same mixture behavior in the form of λ_c values shifted towards the hydrogenated species was also reported by Berger Bioucas et al. [15] for the mixtures of H0-DPM/H12-DPM. This trend for λ_c indicates again that the intermolecular forces between unlike dehydrogenated and hydrogenated molecules are weaker than between the molecules of the same kind,

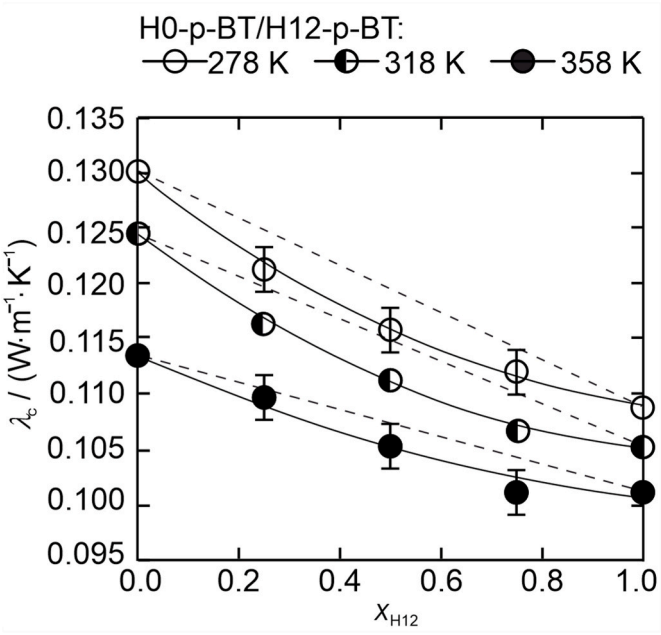

Fig. 5. Experimental thermal conductivity data (symbols) for binary mixtures of H0-p-BT and H12-p-BT as a function of the amount fraction of H12-p-BT, x_{H12}, for three representative T of (278.15, 318.15, and 358.15) K. As a guide for eye, the straight lines (—) represent second-order polynomial fits of the experimental λ_c data as a function of x_{H12}. The dashed lines (– – –) visualize straight lines connecting the experimental λ_c data at $x_{H12} = 0$ and at $x_{H12} = 1$ to indicate a simple linear amount fraction-based mixing rule. Error bars indicating the expanded ($k = 2$) uncertainty of the experimental λ_c data are only shown for exemplary state points.

which is in accordance with the behavior described before for ρ and V_m^E in chapter 3.2. Interestingly, also the liquid viscosity as a further transport property besides λ_c has shown negative deviations from a linear mixing for H0-DPM/H12-DPM mixtures [16]. This could be due to the chemical differences between aromatic benzene rings and non-aromatic cyclohexyl rings. In related binary mixtures of H0-BT and H12-BT, molecules with easily polarizable and planar phenyl rings [60,61,65] and those with less polarizable non-polar cyclohexyl rings of bulkier three-dimensional structure [60,61] are present. Electrostatic interactions among the H0-BT aromatic rings by, for example, π-π-stacking or edge-to-face interactions [55] will be much more preferable than between H0-BT and the non-polar H12-BT molecules, which also tend to interact rather with each other than with H0-BT. This relatively weak interaction between the unlike dehydrogenated and hydrogenated species appears to slightly perturb the transport due to heat conduction that is governed by vibrational and translational modes at low T, as discussed in section 3.3.2. However, a more dedicated analysis of this mixture behavior is not possible since no theoretical model can capture the relevant mechanisms of heat conduction in liquids at T far away from the boiling point.

For all studied T, the experimental data for λ_c of the single binary mixture of H0-o-BT and oxo-H0-o-BT with $x_{H0\text{-}o\text{-}BT} = 0.483$ agree with the measurement results for the pure substances within single uncertainties. This behavior indicates no clear deviations from a linear amount fraction-based mixing rule in the case of the dehydrogenated/oxygenated LOHC pairs.

Although the deviations of the experimental data for λ_c of the H0-BT/H12-BT mixtures from a linear mixing rule are relatively small within about 3 %, the observed non-linear behavior may have non-negligible implications on the process design. Since λ_c affects the overall heat transfer coefficient in the hydrogenation and dehydrogenation units, overestimations in λ_c by 3 % caused by the simplified use of a linear mixing rule may lead to underestimations in the heat transfer areas in a similar order of magnitude. This may result in slightly increased operation costs in the form of, e.g., increased pressure losses due to pumping. Therefore, the experimental information on the behavior of λ_c of the H0-BT/H12-BT mixtures is of relevance for a proper design of LOHC processes and apparatuses.

3.3.4. *Application of prediction model for cyclic hydrocarbons*

The experimental data for the nine pure regioisomers studied in this work are used to test a prediction model for λ_c for cyclic hydrocarbons at atmospheric p suggested by Berger Bioucas et al. [15]. In this study, all relevant details of the model $\lambda_{c,pred}$ can be found. It requires only the molar mass M and T-dependent density data $\rho(T)$ as input parameters, and includes three fit parameters A, B, and C. The latter parameter C was optimized to 2.2 and 2.0 for selected dehydrogenated and hydrogenated components. For the oxo-H0-BT regioisomers, which were not part of the training set in Ref. [15], $C = 2.2$ is used in the present work. For $\rho(T)$, Eq. (4) based on the present measurements is employed.

Fig. 6 shows the relative deviations of the experimental λ_c data measured in this work from the corresponding predictions $\lambda_{c,pred}$ for all regioisomers of H0-BT, H12-BT, and oxo-H0-BT as a function of T. It can be seen that the model overestimates the experimental results in all cases. A sound representation is given for the three regioisomers of H0-BT and H12-BT, where the deviations of λ_c from $\lambda_{c,pred}$ are within −10 % and, in most cases, within −5 %. Among these regioisomers, the largest deviations are found for H0-o-BT, which can be related to its relatively large ρ, which results in relatively large predicted $\lambda_{c,pred}$ values. The significantly worse representation of λ_c is observed for all oxo-H0-BT regioisomers. Here, the deviations of λ_c from $\lambda_{c,pred}$ cover a range from −15.2 % at $T = 278.15$ K to −8.9 % at $T = 358.15$ K. The observations made for the present regioisomers are reasonable considering the sources used to develop the prediction model [15]. The measurement results for the technical mixtures of dehydrogenated H0-BT and hydrogenated H12-BT reported by Berger Bioucas et al. [15] and shown in Fig. 4 were a main part of the training set. Since these data tend to show too large λ_c especially at low T, it is plausible that the prediction model gives overestimations compared to the present more reliable λ_c results in this T range. Moreover, the fifteen further types of cyclic hydrocarbons, like benzene, toluene, cyclohexane, and methylcyclohexane, considered as fluids in the model development did not include substances with heteroatoms such as oxygen, as it is given by the oxo-H0-BT regioisomers. The latter contain a relatively strong polar carbonyl group, which may enable to form relatively strong electrostatic interactions such as induced dipole-dipole interactions with the phenyl ring. It seems that such interactions are not represented well in the model with the fit parameters A, B, and C that were optimized against a set of weakly polar substances. Therefore, it can be expected that the model cannot represent λ_c for the partially oxidized derivatives of H0-BT. To tackle this, a further improvement of the prediction model by

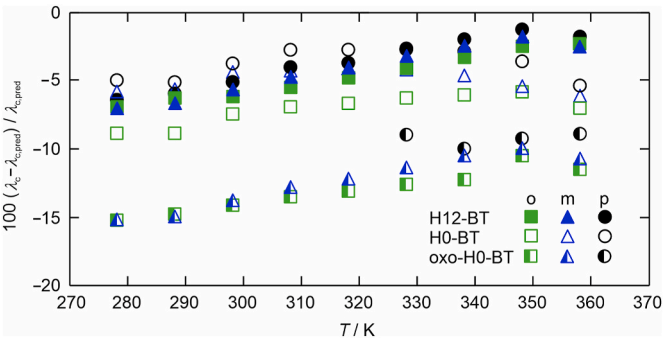

Fig. 6. Relative deviation of the measured thermal conductivity data of the regioisomers of H0-BT, H12-BT, and oxo-H0-BT determined in this work from the prediction model described by Berger Bioucas et al. [15] as a function of T.

including further variables such as dipole moment would be required, which is out of the scope of the present work since also a much larger database for various similar substance types would be required.

For the two selected ortho-based substances H0-o-BT and H12-o-BT where the prediction model [15] works has shown to work quite well, $\lambda_{c,pred}$ was exemplarily calculated at LOHC process-relevant T of 523.15 K. For this, the required ρ data at 523.15 K were taken from the T-dependent correlations developed in Ref. [16] up to 473.15 K. Values for $\lambda_{c,pred}$ of 0.096 $W{\cdot}m^{-1}{\cdot}K^{-1}$ for H0-o-BT and 0.086 $W{\cdot}m^{-1}{\cdot}K^{-1}$ for H12-o-BT at 523.15 K agree well with the extrapolated λ_c values reported in section 3.3.2 with relative deviations of (6.5 and −4.6) %. This shows that the suggested prediction model [15] allows to provide reliable estimations for λ_c of dehydrogenated and hydrogenated BT-based substances up to elevated T within about ±10 %.

4. Conclusions

In the present study, the thermal conductivity of the relevant compounds in the benzyltoluene-based LOHC system has been investigated. A particular focus was to study the influence of regioisomerism of the dehydrogenated, hydrogenated, and partially oxygenated substances on λ_c, which is an important thermophysical property for LOHC processes involving the autothermal concept. A reliable experimental database for λ_c from (278.15–358.15) K could be determined at atmospheric pressure by applying a steady-state guarded parallel-plate instrument, which enables an absolute measurement with an expanded relative uncertainty $U_r(\lambda_c) = 0.02$. Supplementary measurements of the refractive index and the density ρ, for which new data were provided for the pure oxo-H0-BT regioisomers, enabled to evaluate the experimental results and a prediction model for λ_c as well as to derive structure-property relationships. Positive excess molar volumes for selected H0-BT/H12-BT mixtures up to 1.0 $cm^3{\cdot}mol^{-1}$ indicate weak interactions between unlike species, while H0-BT/oxo-H0-BT mixtures show distinctly smaller values. The oxo-H0-BT regioisomers show overall the largest values for λ_c, which are similar to those of the H0-BT regioisomers and significantly larger than those of the H12-BT ones. For all three classes, the effect of the regioisomerism on λ_c is relatively small, taking into consideration the agreement of the measurement data within combined uncertainties. Furthermore, the experimental results for mixtures of H0-BT in mixtures with H12-BT or oxo-H0-BT revealed a non-linear behavior for λ_c as a function of amount fraction for the first mixture type, while matching values within the uncertainties were found for the second type. All experimental data were compared to available data in the literature which are very scarce so far, especially for λ_c. The application of an available prediction model for λ_c of cyclic hydrocarbons using information on the density and molar mass indicated sound agreement with the T-dependent measurement data for the H0-BT and H12-BT regioisomers, which allows realistic predictions at T up to process-relevant values of 523 K and above. However, the model cannot represent λ_c of the oxo-H0-BT regioisomers since this partially oxygenated fluid class has not been part of the substances used in the model development.

CRediT authorship contribution statement

Hubert P. Blabus: Writing – review & editing, Writing – original draft, Investigation, Formal analysis. **Francisco E. Berger Bioucas:** Writing – review & editing, Investigation. **Michael H. Rausch:** Writing – review & editing, Supervision, Project administration, Conceptualization. **Thomas M. Koller:** Writing – review & editing, Supervision, Project administration, Conceptualization. **Peter Wasserscheid:** Writing – review & editing, Project administration. **Andreas P. Fröba:** Writing – review & editing, Supervision, Project administration, Funding acquisition, Conceptualization.

Funding sources

This work was funded by the Bavarian Ministry of Economic Affairs, Regional Development and Energy.

Declaration of competing interest

The authors declare that they have no known competing financial interests or personal relationships that could have appeared to influence the work reported in this paper.

Acknowledgments

The authors gratefully acknowledge funding of the Erlangen Graduate School of Advanced Optical Technologies by the Bavarian State Ministry for Science and Art.

Appendix A. Supplementary data

Supplementary data to this article can be found online at https://doi.org/10.1016/j.ijhydene.2025.152973.

References

[1] Dudin MN, Frolova EE, Protopopova OV, Mamedov O, Odintsov SV. Study of innovative technologies in the energy industry: nontraditional and renewable energy sources. JESI 2019;6(11):1704–13. https://doi.org/10.9770/jesi.2019.6.4.
[2] Potrč S, Čuček L, Martin M, Kravanja Z. Sustainable renewable energy supply networks optimization – the gradual transition to a renewable energy system within the European Union by 2050. Renew Sustain Energy Rev 2021;146:111186. https://doi.org/10.1016/j.rser.2021.111186.
[3] Erdiwansyah Mahidin, Husin H, Nasaruddin. Zaki M,Muhibbuddin. A critical review of the integration of renewable energy sources with various technologies. Protection and Control of Modern Power. Systems 2021;6:1–18. https://doi.org/10.1186/s41601-021-00181-3.
[4] Preuster P, Alekseev A, Wasserscheid P. Hydrogen storage technologies for future energy systems. Annu Rev Chem Biomol Eng 2017;8:445–71. https://doi.org/10.1146/annurev-chembioeng-060816-101334.
[5] Mahlia TMI, Saktisahdan TJ, Jannifar A, Hasan MH, Matseelar HSC. A review of available methods and development on energy storage; technology update. Renew Sustain Energy Rev 2014;33:532–45. https://doi.org/10.1016/j.rser.2014.01.068.
[6] Rao PC, Yoon M. Potential liquid-organic hydrogen carrier (LOHC) systems: a review on recent progress. Energies 2020;13:6040. https://doi.org/10.3390/en13226040.
[7] Niermann M, Beckendorff A, Kaltschmitt M, Bonhoff K. Liquid Organic Hydrogen Carrier (LOHC) – assessment based on chemical and economic properties. Int J Hydrogen Energy 2019;44:6631–54. https://doi.org/10.1016/j.ijhydene.2019.01.199.
[8] Markiewicz M, Zhang Y Q, Bösmann A, Brückner N, Thöming J, Wasserscheid P, et al. Environmental and health impact assessment of Liquid Organic Hydrogen Carrier (LOHC) systems – challenges and preliminary results. Energy Environ Sci 2015;8:1035–45. https://doi.org/10.1039/C4EE03528C.
[9] Geburtig D, Preuster P, Bösmann A, Müller K, Wasserscheid P. Chemical utilization of hydrogen from fluctuating energy sources – catalytic transfer hydrogenation from charged Liquid Organic Hydrogen Carrier systems. Int J Hydrogen Energy 2016;41:1010–7. https://doi.org/10.1016/j.ijhydene.2015.10.013.
[10] Teichmann D, Arlt W, Schlücker E, Wasserscheid P. Transport and storage of hydrogen via Liquid Organic Hydrogen Carrier (LOHC) systems. Hydrogen science and engineering : materials, processes, systems and technology. John Wiley & Sons, Ltd; 2016. p. 811–30. https://doi.org/10.1002/9783527674268.ch33.
[11] Preuster P, Papp C, Wasserscheid P. Liquid organic hydrogen carriers (LOHCs): toward a hydrogen-free hydrogen economy. Acc Chem Res 2017;50:74–85. https://doi.org/10.1021/acs.accounts.6b00474.
[12] Siegert F, Gundermann M, Maurer L, Hahn S, Hofmann J, Distel M, et al. Autothermal hydrogen release from liquid organic hydrogen carrier systems. Int J Hydrogen Energy 2024;91:834–42. https://doi.org/10.1016/j.ijhydene.2024.10.044.
[13] Brückner N, Obesser K, Bösmann A, Teichmann D, Arlt W, Dungs J, et al. Evaluation of industrially applied heat-transfer fluids as liquid organic hydrogen carrier systems. ChemSusChem 2014;7:229–35. https://doi.org/10.1002/cssc.201300426.
[14] Shi L, Qi S, Qu J, Che T, Yi C, Yang B. Integration of hydrogenation and dehydrogenation based on dibenzyltoluene as liquid organic hydrogen energy carrier. Int J Hydrogen Energy 2018;44. https://doi.org/10.1016/j.ijhydene.2018.09.083.
[15] Berger Bioucas FE, Piszko M, Kerscher M, Preuster P, Rausch MH, Koller TM, et al. Thermal conductivity of hydrocarbon liquid organic hydrogen carrier systems: measurement and prediction. J Chem Eng Data 2020;65:5003–17. https://doi.org/10.1021/acs.jced.0c00613.

[16] Kerscher M, Jander JH, Cui J, Maurer LA, Wolf P, Hofmann JD, et al. Thermophysical properties of the liquid organic hydrogen carrier system based on benzyltoluene considering influences of isomerism and dissolved hydrogen. Int J Hydrogen Energy 2024;77:1009–25. https://doi.org/10.1016/j.ijhydene.2024.06.131.

[17] Rüde T, Dürr S, Preuster P, Wolf M, Wasserscheid P. Benzyltoluene/perhydro benzyltoluene – pushing the performance limits of pure hydrocarbon liquid organic hydrogen carrier (LOHC) systems. Sustain Energy Fuels 2022;6:1541–53. https://doi.org/10.1039/D1SE01767E.

[18] Aslam R, Khan MH, Ishaq M, Müller K. Thermophysical studies of dibenzyltoluene and its partially and fully hydrogenated derivatives. J Chem Eng Data 2018;63:4580–7. https://doi.org/10.1021/acs.jced.8b00652.

[19] Jess A, Wasserscheid P. Chemical technology. second ed. Weinheim: Wiley-VCH; 2020.

[20] Caputo AC, Federici A, Pelagagge PM, Salini P. On the design of shell-and-tube heat exchangers under uncertain operating conditions. Appl Therm Eng 2022;212:118541. https://doi.org/10.1016/j.applthermaleng.2022.118541.

[21] Koniorczyk M, Grymin W. Influence of the thermal conductivity and ambient temperature uncertainty on the heat losses through the external Wall. Buildings 2021;11:84. https://doi.org/10.3390/buildings11030084.

[22] Paul G, Chopkar M, Manna I, Das PK. Techniques for measuring the thermal conductivity of nanofluids: a review. Renew Sustain Energy Rev 2010;14:1913–24. https://doi.org/10.1016/j.rser.2010.03.017.

[23] Berger Bioucas FE, Rausch MH, Koller TM, Fröba AP. Guarded parallel-plate instrument for the determination of the thermal conductivity of gases, liquids, solids, and heterogeneous systems. Int J Heat Mass Tran 2023;212:124283. https://doi.org/10.1016/j.ijheatmasstransfer.2023.124283.

[24] Wakeham WA, Nagashima A, Sengers JV. International union of pure and applied chemistry. In: Measurement of the transport properties of fluids. Oxford [England] ; Boston : Boca Raton, Fla: Blackwell Scientific Publications; 1991. Distributed in the USA and North America by CRC Press.

[25] Berger Bioucas FE, Koller TM, Fröba AP. Thermal conductivity of glycerol at atmospheric pressure between 268 K and 363 K by using a steady-state parallel-plate instrument. Int J Thermophys 2024;45:52. https://doi.org/10.1007/s10765-024-03347-x.

[26] Berger Bioucas FE, Rausch MH, Schmidt J, Bück A, Koller TM, Fröba AP. Effective thermal conductivity of nanofluids: measurement and prediction. Int J Thermophys 2020;41:55. https://doi.org/10.1007/s10765-020-2621-2.

[27] Berger Bioucas FE, Wu W, Stiegler LMS, Peukert W, Walter J, Adschiri T, et al. Effective thermal conductivity of cyclohexane-based nanofluids containing cerium dioxide nanoparticles with chemisorbed organic shell. Int J Thermophys 2024;46:12. https://doi.org/10.1007/s10765-024-03480-7.

[28] Berger Bioucas FE, Koller TM, Fröba AP. Effective thermal conductivity of nanofluids containing silicon dioxide, titanium dioxide, copper oxide, polystyrene, or polymethylmethacrylate nanoparticles dispersed in water, ethylene glycol, or glycerol. Int J Thermophys 2025;46:27. https://doi.org/10.1007/s10765-024-03488-z.

[29] Berger Bioucas FE, Koller TM, Fröba AP. Effective thermal conductivity, effective viscosity, and particle diffusion coefficient of microemulsions consisting of water, *n*-decane, and a non-ionic surfactant in different regions of the phase diagram. Int J Heat Mass Tran 2024;232:125901. https://doi.org/10.1016/j.ijheatmasstransfer.2024.125901.

[30] BergerBioucas FE, Koller TM, Fröba AP. Effective thermal conductivity of microemulsions consisting of water micelles in *n*-decane. Int J Heat Mass Tran 2023;200:123526. https://doi.org/10.1016/j.ijheatmasstransfer.2022.123526.

[31] McLaughlin E. The thermal conductivity of liquids and dense gases. Chem Rev 1964;64:389–428. https://doi.org/10.1021/cr60230a003.

[32] Baroncini C, Di Filippo P, Latini G, Pacetti M. Organic liquid thermal conductivity: a prediction method in the reduced temperature range 0.3 to 0.8. Int J Thermophys 1981;2:21–38. https://doi.org/10.1007/BF00503572.

[33] Zhang N, Wang Z. Review of soil thermal conductivity and predictive models. Int J Therm Sci 2017;117:172–83. https://doi.org/10.1016/j.ijthermalsci.2017.03.013.

[34] Sastri SRS, Rao KK. A new temperature–thermal conductivity relationship for predicting saturated liquid thermal conductivity. Chem Eng J 1999;74:161–9. https://doi.org/10.1016/S1385-8947(99)00046-7.

[35] Fröba AP, Rausch MH, Krzeminski K, Assenbaum D, Wasserscheid P, Leipertz A. Thermal conductivity of ionic liquids: measurement and prediction. Int J Thermophys 2010;31:2059–77. https://doi.org/10.1007/s10765-010-0889-3.

[36] Koller TM, Schmid SR, Sachnov SJ, Rausch MH, Wasserscheid P, Fröba AP. Measurement and prediction of the thermal conductivity of tricyanomethanide- and tetracyanoborate-based imidazolium ionic liquids. Int J Thermophys 2014;35:195–217. https://doi.org/10.1007/s10765-014-1617-1.

[37] Kerscher M, Jander JH, Cui J, Maurer LA, Wolf P, Hofmann JD, et al. Thermophysical properties of the liquid organic hydrogen carrier system based on benzyltoluene considering influences of isomerism and dissolved hydrogen. Int J Hydrogen Energy 2024;77:1009–25. https://doi.org/10.1016/j.ijhydene.2024.06.131.

[38] Rüde T, Dürr S, Preuster P, Wolf M, Wasserscheid P. Benzyltoluene/perhydro benzyltoluene – pushing the performance limits of pure hydrocarbon liquid organic hydrogen carrier (LOHC) systems. Sustain Energy Fuels 2022;6:1541–53. https://doi.org/10.1039/D1SE01767E.

[39] Braun R, Fischer S, Schaber A. Elimination of the radiant component of measured liquid thermal conductivities. Wärme- und Stoffübertragung 1983;17:121–4. https://doi.org/10.1007/BF01007228.

[40] Poltz H. Die Wärmeleitfähigkeit von Flüssigkeiten II: Der Strahlungsanteil der effektiven Wärmeleitfähigkeit. Int J Heat Mass Tran 1965;8:515–27. https://doi.org/10.1016/0017-9310(65)90042-6.

[41] Kohler M. Einfluß der Strahlung auf den Wärmetransport durch eine Flüssigkeitsschicht. ZEITSCHRIFT FUR ANGEWANDTE PHYSIK 1965;18:356.

[42] Huber ML, Perkins RA, Friend DG, Sengers JV, Assael MJ, Metaxa IN, et al. New international formulation for the thermal conductivity of H2O. J Phys Chem Ref Data 2012;41. https://doi.org/10.1063/1.4738955.

[43] Lemmon EW, Bell IH, Huber ML, McLinden MO. REFPROP, Standard Reference Data Program. 2018. version 10.0.

[44] Rüde T, Lu Y, Anschütz L, Blasius M, Wolf M, Preuster P, et al. Performance of continuous hydrogen production from perhydro benzyltoluene by catalytic distillation and heat integration concepts with a fuel cell. Energy Technol 2023;11:2201366. https://doi.org/10.1002/ente.202201366.

[45] González B, Domínguez I, González EJ, Domínguez Á. Density, speed of sound, and refractive index of the binary systems cyclohexane (1) or methylcyclohexane (1) or cyclo-octane (1) with benzene (2), toluene (2), and ethylbenzene (2) at two temperatures. J Chem Eng Data 2010;55:1003–11. https://doi.org/10.1021/je900468u.

[46] Berland K, Cooper VR, Lee K, Schröder E, Thonhauser T, Hyldgaard P, et al. van der Waals forces in density functional theory: a review of the vdW-DF method. Rep Prog Phys 2015;78:066501. https://doi.org/10.1088/0034-4885/78/6/066501.

[47] Haynes WM, editor. CRC handbook of chemistry and physics. 97th ed. Boca Raton: CRC Press; 2016. https://doi.org/10.1201/9781315380476.

[48] Mahl BS, Kaur H, Singh H, Khurma JR. Thermodynamic properties of some binary mixtures containing carbonyl compounds. Thermochim Acta 1986;99:291–7. https://doi.org/10.1016/0040-6031(86)85291-1.

[49] Kerscher M, Jander JH, Cui J, Martin MM, Wolf M, Preuster P, et al. Viscosity, surface tension, and density of binary mixtures of the liquid organic hydrogen carrier diphenylmethane with benzophenone. Int J Hydrogen Energy 2022;47:15789–806. https://doi.org/10.1016/j.ijhydene.2022.03.051.

[50] Natarajan V, Arivanandhan M, Anandan P, Sankaranarayanan K, Ravi G, Inatomi Y, et al. In-situ observation of faceted growth of benzophenone single crystals. Mater Chem Phys 2014;144:402–8. https://doi.org/10.1016/j.matchemphys.2014.01.010.

[51] Wang W, Lin X, Huang W. The optical properties of benzophenone crystal grown from undercooled melt with oriented growth method. Opt Mater 2007;29:1063–5. https://doi.org/10.1016/j.optmat.2006.04.005.

[52] Graham DJ, Magdolinos P, Tosi M. Investigation of solidification of benzophenone in the supercooled liquid State. J Phys Chem 1995;99:4757–62. https://doi.org/10.1021/j100013a053.

[53] Schmidt PS, Kerscher M, Klein T, Jander JH, Berger Bioucas FE, Rüde T, et al. Effect of the degree of hydrogenation on the viscosity, surface tension, and density of the liquid organic hydrogen carrier system based on diphenylmethane. Int J Hydrogen Energy 2022;47:6111–30. https://doi.org/10.1016/j.ijhydene.2021.11.198.

[54] Kumaran MK, Benson GC. Excess molar volumes of (benzene + cyclohexane) at 323.15 K. J Chem Therm 1984;16:183–7. https://doi.org/10.1016/0021-9614(84)90153-8.

[55] Meyer EA, Castellano RK, Diederich F. Interactions with aromatic rings in chemical and biological recognition. Angew Chem Int Ed 2003;42:1210–50. https://doi.org/10.1002/anie.200390319.

[56] Zhao AZ, Garay JE. High temperature liquid thermal conductivity: a review of measurement techniques, theoretical understanding, and energy applications. Prog Mater Sci 2023;139:101180. https://doi.org/10.1016/j.pmatsci.2023.101180.

[57] Khrapak SA, Khrapak AG. Vibrational model for thermal conductivity of Lennard-Jones fluids: applicability domain and accuracy level. Phys Rev E 2023;108:064129. https://doi.org/10.1103/PhysRevE.108.064129.

[58] Bridgman PW. The thermal conductivity of liquids under pressure. Proc Am Acad Arts Sci 1923;59:141–69. https://doi.org/10.2307/20026073.

[59] Watanabe H, Kato H. Thermal conductivity and thermal diffusivity of twenty-nine liquids: alkenes, cyclic (alkanes, alkenes, alkadienes, aromatics), and deuterated hydrocarbons. J Chem Eng Data 2004;49:809–25. https://doi.org/10.1021/je034162x.

[60] Beg SA, Tukur NM, Al-Harbi DK, Hamad E. Densities and excess volumes of the benzene-cyclohexane system between 298.15 and 473.15 K. Fluid Phase Equilib 1994;94:289–300. https://doi.org/10.1016/0378-3812(94)87063-2.

[61] Jonas J, Hasha D, Huang SG. Density effects of transport properties in liquid cyclohexane. J Phys Chem 1980;84:109–12. https://doi.org/10.1021/j100438a024.

[62] Eastman, Marlotherm LH. Data sheet of heat trasfer fluid. 2022.

[63] Taxis B, Zalaf M, Wakeham WA. Thermal conductivity and thermal diffusivity of xylene isomers in the temperature range 308-360 K at pressures up to 0.38 GPa. Int J Thermophys 1988;9:21–35. https://doi.org/10.1007/BF00503997.

[64] Rausch MH, Krzeminski K, Leipertz A, Fröba AP. A new guarded parallel-plate instrument for the measurement of the thermal conductivity of fluids and solids - ScienceDirect. Int J Heat Mass Tran 2013;58:610–8. https://doi.org/10.1016/j.ijheatmasstransfer.2012.11.069.

[65] Kanai H, Inouye V, Yazawa L, Goo R, Wakatsuki H. Importance of debye and keesom interactions in separating m-xylene and p-xylene in GC-MS analysis utilizing PEG stationary phase. Journal of Chromatographic Science 2005;43:57–62. https://doi.org/10.1093/chromsci/43.2.57.